Title

Colicin E1 opens its hinge to plug TolC

Authors

S. Jimmy Budiardjo[1], Jacqueline J. Stevens[2], Anna L. Calkins[3], Ayotunde P. Ikujuni[2], Virangika K. Wimalasena[2], Emre Firlar[4], David A. Case[5], Julie S. Biteen[3], Jason T. Kaelber[4] and Joanna S.G. Slusky[1,2,*]

Affiliations

[1] Center for Computational Biology, The University of Kansas, 2030 Becker Dr., Lawrence, KS 66047.

[2] Department of Molecular Biosciences, The University of Kansas, 1200 Sunnyside Ave. Lawrence KS 66045.

[3] Department of Chemistry, University of Michigan, Ann Arbor MI 48109-1055.

[4] Rutgers CryoEM & Nanoimaging Facility and Institute for Quantitative Biomedicine, Rutgers University, Piscataway, NJ 08854, USA.

[5] Department of Chemistry and Chemical Biology, Rutgers University, Piscataway, NJ 08854 USA.

*Correspondence: slusky@ku.edu.

Abstract

The double membrane architecture of Gram-negative bacteria forms a barrier that is effectively impermeable to extracellular threats. Bacteriocin proteins evolved to exploit the accessible, surface-exposed proteins embedded in the outer membrane to deliver cytotoxic cargo. Colicin E1 is a bacteriocin produced by, and lethal to, *Escherichia coli* that hijacks the outer membrane proteins TolC and BtuB to enter the cell. Here we capture the colicin E1 translocation domain inside its membrane receptor, TolC, by high-resolution cryoEM, the first reported structure of a bacteriocin bound to TolC. Colicin E1 binds stably to TolC as an open hinge through the TolC pore—an architectural rearrangement from colicin E1's unbound conformation.

This binding is stable in live *E. coli* cells as indicated by single-molecule fluorescence microscopy. Finally, colicin E1 fragments binding to TolC plugs the channel, inhibiting its native efflux function as an antibiotic efflux pump and heightening susceptibility to three antibiotic classes. In addition to demonstrating that these protein fragments are useful starting points for developing novel antibiotic potentiators, this method could be expanded to other colicins to inhibit other outer membrane protein functions.

Introduction

In Gram-negative bacteria, the concentric structures of the outer membrane, cell wall, and cytoplasmic membrane protect the cell from extracellular threats. Of these protective structures, the outer membrane forms a particularly formidable barrier(*5*), owing to the impermeability of the lipopolysaccharide (LPS) layer that constitutes the outer membrane(*7*). The primary means by which external molecules can gain access to the cell is through the ~100 varieties of barrel-shaped proteins that are embedded in each bacterium outer membrane(*8*) and whose diverse functions include the transport of molecules across the membrane—specifically, the import of nutrients and metabolites and the export of toxins and waste.

Because outer membrane proteins (OMPs) are accessible from outside the cell, bacteriophage and bacterial toxins have evolved to exploit OMPs to initiate delivering cargo across the outer membrane. Bacteriocins hijack the OMPs of a target bacterium to cross its impermeable outer membrane and kill the bacterium. Colicins are *E. coli*-specific bacteriocins, protein toxin systems through which bacteria engage in bacterial warfare with other, similar bacteria. Although colicins differ in their receptor targets and killing mechanisms, most colicins share a common tri-domain architecture, comprising the following components: (i) an N-terminal translocation (T) domain, (ii) a receptor-binding (R) domain, and (iii) a C-terminal cytotoxic (C) domain (Figure 1A). Much of what is known of E colicin import has been determined through studies of the colicin E3 and E9 as reviewed by Cramer et al.(*9*) Import is initialized by R domain

62 binding to the vitamin B12 transporter, BtuB, with high affinity(*10, 11*); this binding localizes the
63 colicin onto the outer membrane. Once the colicin is tethered to the outer membrane surface, the
64 T domain initiates translocation using the secondary OMP receptor OmpF to access TolA/Pal
65 system for group A colicins or the Ton system group B colicins. In most cases, the T domain
66 requires an OMP distinct from the R domain target.(*12*) A handful of colicins have been
67 structurally characterized with their OMP counterparts, although not in their entirety. Previous
68 structures of short N-terminal fragments of the T domain of ColE9 with OmpF(*13*) and the The R
69 domains of ColE2/E3 and Ia with BtuB(*11, 14*) and Cir(*10*), respectively showed that T domains
70 fully penetrate deeply into lumen of the outer membrane receptors while R domains interact with
71 the extracellular loop regions of their receptors. Studies of the bacteriocin pyocin S5 from
72 *Pseudomonas aeruginosa* suggest that bacteriocin architectures and mechanisms may be
73 conserved across all Gram-negative species.

74 Colicin E1 is a bacteriocin secreted by *E. coli* that enters the periplasm of neighboring
75 cells and forms a pore on the cytoplasmic membrane leading to membrane depolarization and cell
76 death. Colicin E1 uses TolC, the outer membrane component of the acridine efflux pump, as the T
77 domain receptor(*15*) and BtuB as the R domain receptor(*16*). A high-resolution x-ray structure
78 exists of only the cytotoxic domain of colicin E1(*17*) but not the T or R domains, thus no
79 mechanistic insights can be gained about initial steps of import. Domain swapping experiments
80 (*15*) between colicin A and E1 identified regions of the protein that interact with specific outer
81 membrane proteins. Early studies of pore forming colicins, including E1, showed that cytotoxic-
82 domain-induced K^+ efflux on the inner membrane can be reversed after it has begun by
83 subsequent addition of trypsin to cells. This, in addition to trypsin's inability to cross the outer
84 membrane, led to the belief that portions of colicin remain tethered to their OMP partners as the
85 cytotoxic domain depolarizes the cytoplasmic membrane.(*18-21*)

86 In order to understand the early stages of colicin E1 import, functional studies of
87 truncations of colicin E1 which lack the cytotoxic domain have been characterized *in vitro*.
88 Residues 100-120 of colicin E1 (termed the 'TolC box', Figure 1A) have been shown to be
89 necessary but not sufficient for binding TolC. Peptides that include the TolC box co-elute with
90 TolC(*22*) and disrupt channel conductance(*22, 23*). Moreover, *E. coli* exposure to TolC-box-
91 containing peptides can prevent subsequent binding and cytotoxicity of full-length colicin E1(*24*).
92 Circular dichroism of the T domain indicates that it exists as a helical hairpin (closed hinge) in
93 solution similar to other colicin T domains(*25*) and that the proline at the center of the TolC box
94 forms its apex(*22*). This measurement led to the proposal, known as the "pillar model,"(*22*) that
95 the T domain inserts into the TolC barrel as a helical hairpin where the N and C-termini are
96 pointing to the cell exterior. According to this model, the hairpin stuck in TolC acts as a buttress
97 to facilitate the cytotoxic domain entry directly through the membrane.
98 A competing model for colicin E1 import, known as the "total thread" model(*9, 22*), posits
99 that the protein unfolds and passes through TolC N-terminus-first as an unstructured peptide,
100 followed by refolding in the periplasm. In this model the binding between the intrinsically
101 unstructured colicin N-termini and periplasmic proteins(*24, 26*) creates a pulling force that results
102 in the translocation of the whole colicin.
103 Here we use cryogenic electron microscopy (cryoEM) to solve the first high-resolution
104 structure of a bacteriocin, colicin E1, bound to TolC (*27*). We find that colicin E1 binds stably to
105 TolC, not as a helical hairpin but as a single-pass folded helix with the N-terminus inside the
106 periplasm. Additionally, we find that the colE1 TR domain binds TolC *in vivo* as well. Using
107 single-molecule fluorescence microscopy, we find that colE1-TR, lacking the cytotoxic domain,
108 remains stalled on the outer membrane and does not fully translocate into cells. Lastly, we
109 leverage this stalling of ColE1 to block the native TolC function as an antibiotic efflux pump.
110 Because they are accessible from outside the cell, OMPs are attractive targets for the development

111 of novel antibiotics, and research has begun to reveal the therapeutic potential of interfering with
112 OMP structure and function. Recently, a monoclonal antibody was found to inhibit OMP folding
113 with bactericidal effects(*28*).

114 Here by determining the structure and mechanism of colE1 insertion we establish an
115 alternative approach for targeting OMPs—the development of molecular plugs that block OMP
116 pores. Such plugs would allow for the manipulation of bacterial transport, providing a means of
117 either starving the bacterium by preventing the import of valuable nutrients or poisoning the
118 bacterium by preventing the export of toxins. Through real-time efflux assays, minimum
119 inhibitory concentration (MIC) experiments, we find that colE1-TR and colE1-T are able to
120 inhibit TolC-mediated efflux. We find that this plugging of TolC reduces the amount of
121 antibiotics required to inhibit the bacterial growth—indicating that this colicin E1 fragment
122 reduces the antibiotic resistance conferred by TolC.

123 **Results**
124
125 **CryoEM structure of TolC embedded in nanodiscs**

126 To determine the structural details of colicin E1 binding to TolC, we solved the cryoEM
127 (cryogenic electron microscopy) structure of TolC embedded in nanodiscs with and without
128 added colE1-T (PDB 6WXH and 6WXI, respectively). We recently reported a high-yield TolC
129 preparation by refolding from inclusion bodies(*29*) and inserted refolded TolC into nanodiscs.
130 The cryoEM structure of refolded TolC alone (Figure 1B) is similar to the previously published
131 crystal structures of natively derived TolC alone(*30*) or in complex with hexamminecobalt(*31*)
132 but with more splayed loops at the periplasmic opening (residues 165-175). There was local
133 variation in resolution within the model with lower resolution associated with the

extracellular/periplasmic ends and the nanodisc scaffold protein (Figure 1B). The lower residue resolution at these apertures may indicate dynamics not captured in the x-ray crystal structures.

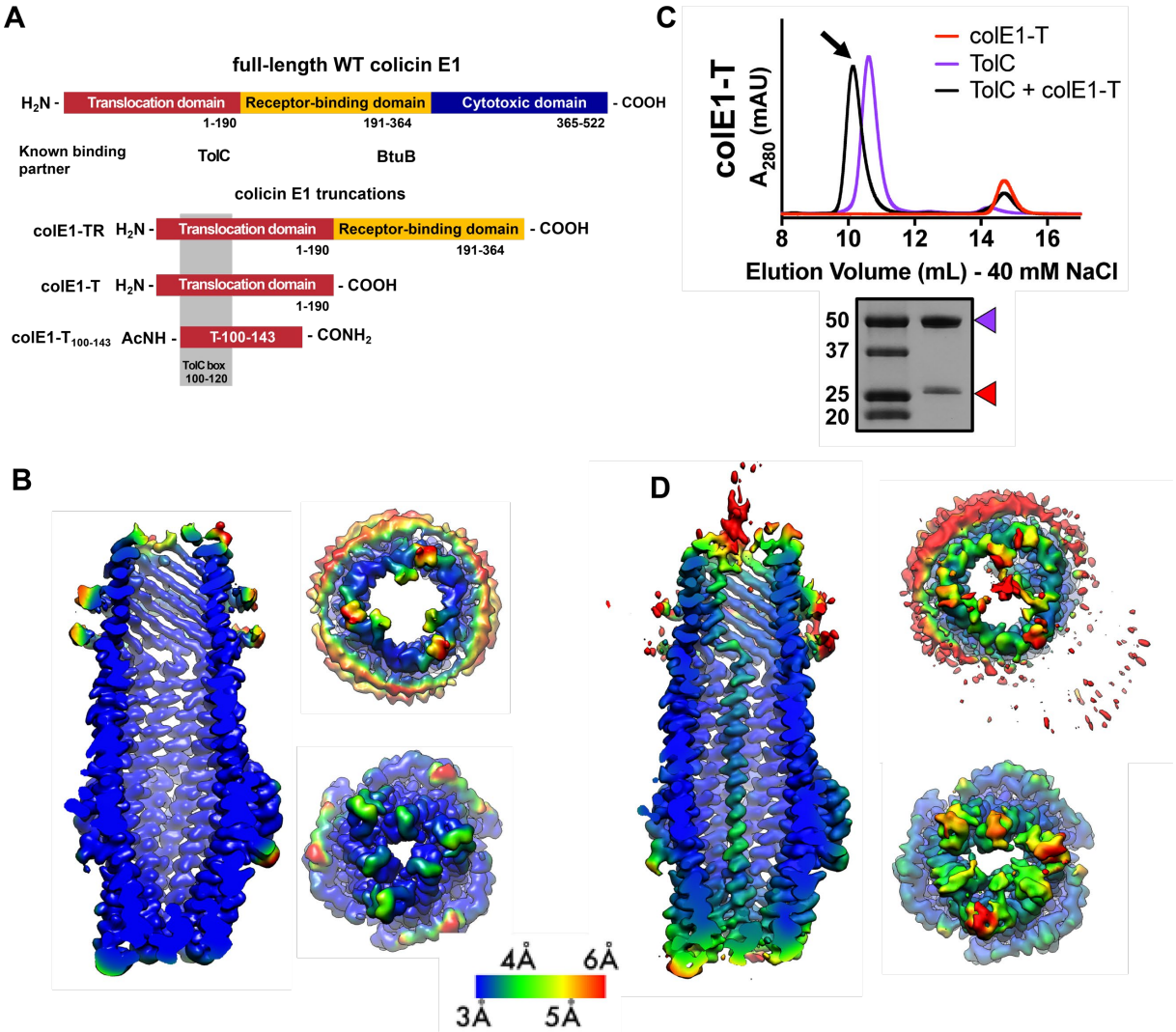

Figure 1. Cell-surface localization of colicin E1 fragments. (**A**) Architecture of full-length colicin E1 showing domains and their known binding partners. Three truncation constructs used in this study (**B**) CryoEM structure of TolC embedded in nanodiscs. Side, top, and bottom views are colored by local resolution, as computed in cryoSPARC from the final half-maps. The side view is cropped to display the particle interior. (**C**) SEC chromatogram of colE1-T (red line) and TolC (purple line). The arrow indicates the co-elution (black line) fractions that were analyzed by SDS-PAGE. On the SDS-PAGE gel (bottom), red arrows indicate the presence of the colicin E1 construct that has co-eluted with TolC. (**D**) The CryoEM structure of colE1-T bound to TolC and colored by local resolution as in (B).

We next determined binding of colicin E1-T domain to capture the complex for structure determination. Residues 1-190 (colE1-T) which span the translocation domain and are known to bind to TolC (Figure 1A). We determined colE1-T:TolC binding *in vitro* via co-elution by size

139 exclusion chromatography (SEC) as previously described(*6*). When colE1-T and TolC were
140 mixed, we observed a leftward shift in the TolC peak and a decrease in intensity associated with
141 the colE1-T peak indicating that a subset of the population has migrated with TolC (Figure 1C).
142 We analyzed the peak (Figure 1C arrow) using SDS-PAGE and found the presence of both colE1-
143 T and TolC. The unimodal shifted peak observed with colE1-T:TolC indicates that there is a
144 single species of fully bound TolC. When resolved by cryoEM, addition of colE1-T to TolC
145 breaks the three-fold channel symmetry and the additional protein is observed running all the way
146 through the TolC barrel as a single-pass, all-α-helical chain spanning more than 130 Å (Figure
147 1D). The maps refined to nominal global resolutions of 2.84 Å and 3.09 Å for the TolC and
148 colE1-T:TolC, respectively (Table S1).

149 The colE1 T domain inserts into TolC with its amino terminus pointing inwards through
150 the periplasmic iris, and 2D class-averages show that the carboxy terminus of the helix continues
151 and projects out into the extracellular space (Figure 2A). 85 of the 190 colE1-T residues could be
152 modeled to this density (residues 46-131) (Figure 2B). No such regular protrusion was seen for
153 the glycine-rich colE1 amino-terminus, which we expect to be disordered in the periplasmic
154 space(*22, 26, 32*). The colE1 chain binds TolC asymmetrically, primarily contacting only one of
155 the three TolC chains.

156 Compared to the unbound state, asymmetric colE1 binding dilates the periplasmic TolC
157 aperture (Figure 2C) and, to a lesser extent, the extracellular aperture (Figure 2D) so that they can
158 accommodate colE1 in the absence of any other proteins or motive force. Although the terminal
159 apertures dilate and are filled by the ligand and the TolC box forms specific interactions with the
160 TolC inner wall, the large internal volume of TolC is not fully occupied by colE1.

161 In solution, unbound colicin E1 is a two-helix hairpin as indicated by far UV circular
162 dichroism (CD)(*6*). A homology model built using I-TASSER(*4*) also predicts the closed hinge
163 conformation with proline 110 at the apex (Figure 2E top). However, our cryoEM reconstruction

of colicin E1 in complex with TolC shows that colE1-T hinges open at the TolC box to an extended conformation upon binding to TolC (Figure 2B, and 2E bottom). The colE1-T helices have a short kink in the middle around proline 110, precisely at the proposed turn location in the hairpin model (Figure 2B inset). This area is also the center of the TolC box that has been known to be critical for the colE1:TolC interaction(*22, 24*).

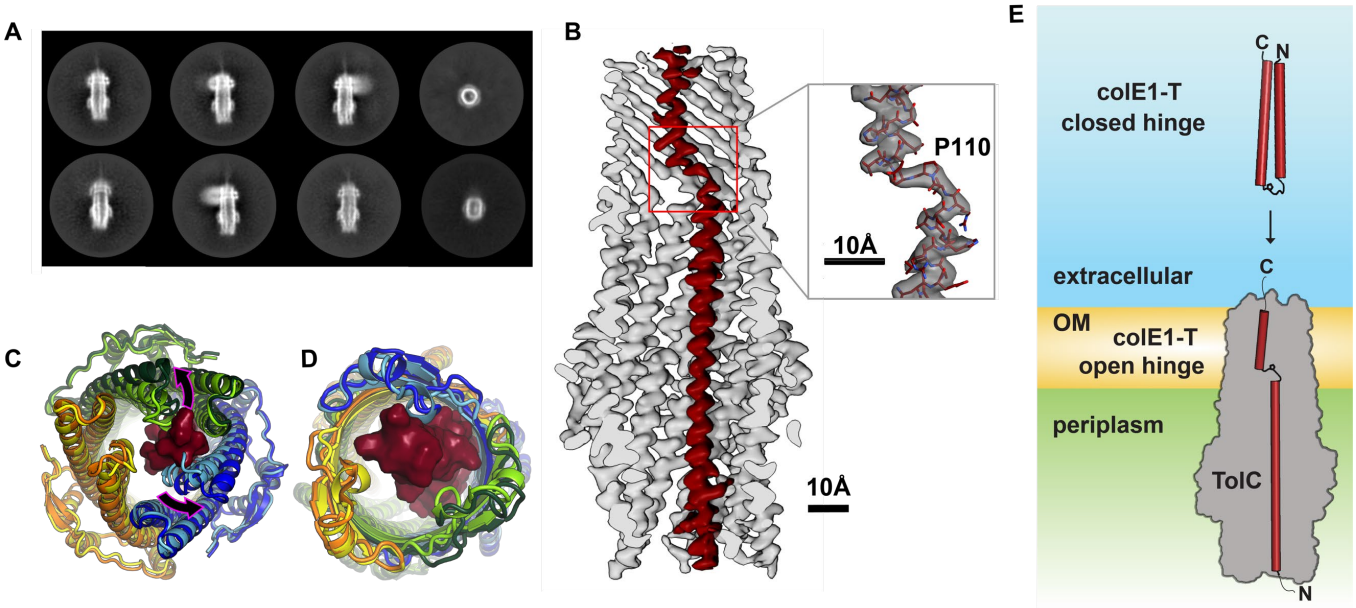

Figure 2. Colicin E1 binds to TolC as a single-pass kinked helix. (**A**) 2D class averages of colE1-T bound to TolC imbedded in nanodiscs (**B**) Cutaway view of the TolC interior (gray). ColE1-T (red) binds asymmetrically in an open-hinge conformation. The hinge region of colE1T including P110 shown in stick representation (inset). (**C** and **D**) The dilated terminal apertures. The apo cryoEM structure of TolC (subunits colored light blue, light green, and yellow) compared to holo cryoEM structure (subunits colored dark blue, dark green and orange). (**C**) Periplasmic aperture. (**D**) Extracellular aperture. (**E**) In the unbound state, colE1-T (red cylinders) exists as a closed hinge. When bound, colE1-T is in an open-hinge conformation through TolC with the N-terminus into the pore of TolC (grey). The homology model of colE1-T in its solution state was built using I-TASSER(*4*) and is consistent with previous experiments(*6*).

Colicin E1 makes residue-specific interactions with TolC

TolC forms a large rigid conduit in the outer membrane and periplasm (Figure 3A) with a water filled lumen. The hydrophilic nature of the channel(*33*) coupled with the inflexibility of the outer-membrane-embedded barrel largely precludes the formation of any hydrophobic interfaces

173 that are typically the basis of protein-protein interfaces involving helical peptides. Yet, we did

174 observe specific polar contacts between colicin E1's TolC box and the TolC barrel.

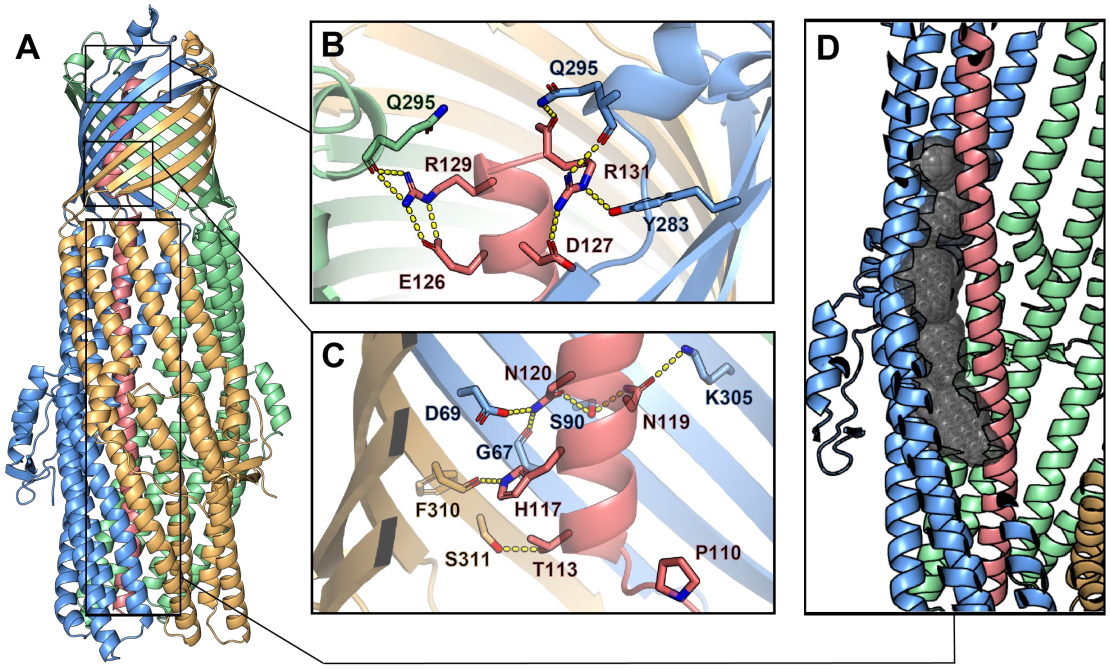

Figure 3. Inter-chain contacts between colE1T and TolC. (**A**) Molecular dynamics simulation refined structure of the colE1-T:TolC complex colored by chain (colE1-T: light red, TolC: light blue, light green, light gold) (**B-C**) Polar interaction network of colE1-T and TolC on the C-terminal side of the proline kink in the β-barrel region. (**B**) near the extracellular opening of TolC and (**C**) before the transition to the TolC periplasmic helical region. Residues involved in forming polar interactions and proline 110 are shown in sticks. (**D**) ColE1-T spanning the TolC helical barrel does not make full contact with the side of the TolC barrel. The cavity (black spheres) between colicin (light red) and one chain of TolC (light blue) was detected using GHECOM(*1-3*)

175 To obtain the most accurate atomic model for interpretation of atomic interactions

176 between peptides, we utilized map-restrained molecular dynamics in model refinement(*34*). The

177 refined model had improved chemical plausibility (for instance, MolProbity(*35*) score improved

178 from 1.25 to 0.50) and polar contact were more easily identified. Because this refinement

179 improved the concordance between the map and model, we conclude that the use of cryoEM

180 density as a restraint was successful in preventing overfitting. Specifically, the EMRinger(*36*)

181 score improved from 2.77 to 3.81 and the map-model FSC=0.5 improved from 3.44Å to 3.37Å.

182 The atomic model showed significant polar interactions form between colicin E1 and
183 TolC at the apertures and around the TolC box. The acidic patch of colicin E1 near the
184 extracellular aperture contains two arginine residues (R129 and R131) that form hydrogen bond
185 networks with one TolC chain each (Figure 3B). In addition, colicin E1 residues T113, A116,
186 N119, N120 (all part of the TolC box) establish polar interactions with TolC residues G67, D69,
187 S90 and K305 on one TolC chain (Figure 3C, light red and light blue) while colicin H117
188 interacts with TolC F310 on a neighboring TolC chain (Figure 3C, light red and light gold). By
189 contrast with the β-barrel of TolC, in the interior of periplasmic helical barrel of TolC, colicin E1
190 does not make full contact with the α-helical barrel interior and there is a gap between the two
191 proteins (Figure 3D). This is in agreement with previous studies that showed a colicin truncation
192 (residues 1-100) that ends just before the beginning of the TolC box does not bind to TolC(*22*) or
193 prevent cytotoxicity of full-length colicin in cells(*24*).
194 Moreover, this structure is consistent with reports that mutations at TolC sites G43 or
195 S257 abrogate colE1 activity(*37*) as these residues are contact sites between TolC and colE1
196 (Figure S1). Conversely, the absence of any effect of mutating colicin R103 and R108(*24*), is
197 consistent with interaction those residues have with the barrel solvent rather than TolC. The
198 newly solved structure, in combination with previous work(*22, 24*), indicates the specificity of
199 colicin E1 binding to TolC is encoded in the portion that binds to TolC β-barrel.
200 **Membrane localization of colE1 truncations**
201 Since we find the colE1 T domain binds to TolC, we investigated if colicin E1 fragments
202 bind to the native TolC in *E. coli* cells. Though ColE1 C domain activity—depolarizing the inner
203 membrane—requires the C domain to pass through the outer membrane(*38*), it remains unclear if
204 the colE1-TR domains translocate as well. We first determined *in vitro* binding of colE1-TR,
205 which includes residues 1-364 (colE1-TR) (Figure 1A) which contains the N-terminal portion that
206 binds to TolC and the C-terminal portion that binds to BtuB. ColE1-TR aggregates at the salt

207 concentration (40 mM) used for the co-elution experiment used for colE1-T so we increased the
208 NaCl concentration to 200 mM. ColE1-T still binds to TolC at 200 mM NaCl although to a much
209 lesser degree (Figure S2). Unlike colE1-T (Figure 1C), colE1-TR shows a bimodal distribution
210 indicative of a mixed population of bound and unbound TolC (Figure 4A). Using an extracellular
211 protease digestion assay, we assessed whether colE1-T and colE1-TR translocate into the cell or
212 localize on the cell surface. ColE1 fragments were incubated with cells, washed, and treated with
213 or without trypsin to digest any extracellularly bound protein to cells. When probing for the C-
214 terminal epitope by immunoblotting, there was no detectible colE1-T binding (Figure 4B, left),
215 though there was detectible binding of ColE1-TR (Figure 4B, right). Moreover, we found that if
216 colE1-TR is incubated with cells and subsequently treated with increasing trypsin concentrations,
217 the colE1-TR band disappeared, indicating that the colicin E1 fragment was localized to the outer
218 membrane surface (Figure 4B, right). The periplasmic control SurA was not degraded at any
219 trypsin concentration unless the cells were lysed before trypsin digestion(*39*).

220 Since the proteolysis experiments are not sensitive enough to detect if only a few
221 molecules have entered the cell, we further probed the interaction between the cell membrane and
222 surface-localized colE1-TR with single-molecule fluorescence microscopy using the fluorescent
223 dye Cy3. This method is able to detect single molecules on the cell surface as well as those within
224 the cell indicative of those molecules having crossed the outer membrane(*40, 41*). When colE1-
225 TR-Cy3 was added to the extracellular environment of WT BW25113 *E. coli* (containing TolC),
226 distinct puncta (Figure 4C, left) formed on 94% of the cells (number of cells, n = 111) (Figure
227 4D); cells with observed puncta most often featured a single punctum, though a small fraction had 2
228 puncta. On average, the WT cells had 1.2 puncta. In a Δ*tolC* strain, puncta were observed on only
229 18% of cells (n = 99) (Figure 4C**,** right; Figure 4D); on average, the Δ*tolC* cells had 0.2 puncta.
230 As a Δ*btuB* control strain, we used BL21 (DE3) which is known to have a premature stop codon
231 at *btuB* residue 58(*42*). Puncta were observed on only 3% of cells lacking BtuB (n = 105) (Figure

232 4D and S3A); on average, the Δ*btuB* cells had 0 puncta. In WT and Δ*tolC* cells that featured

233 puncta, colE1-TR formed puncta consistent with ~20 molecules based on dividing the puncta

234 intensity by the fluorescence intensity of the last fluorescent molecule before photobleaching (*43*).

235 The observed size and number of molecules are in agreement with previous studies of BtuB

236 clusters (*44, 45*) and the punctum locations within the cell were variable. To rule out punctum

237 formation as an artifact of Cy3 conjugation, we found colE1-TR-GFP displayed the same cluster

238 formation as colE1-TR-Cy3 (Figure S3B). No other single protein binding events were detected

239 aside from the puncta on either WT or Δ*tolC* cells.

240 Fluorescently labeled pyocins, the colicin analog in *Pseudomonas*, have previously been

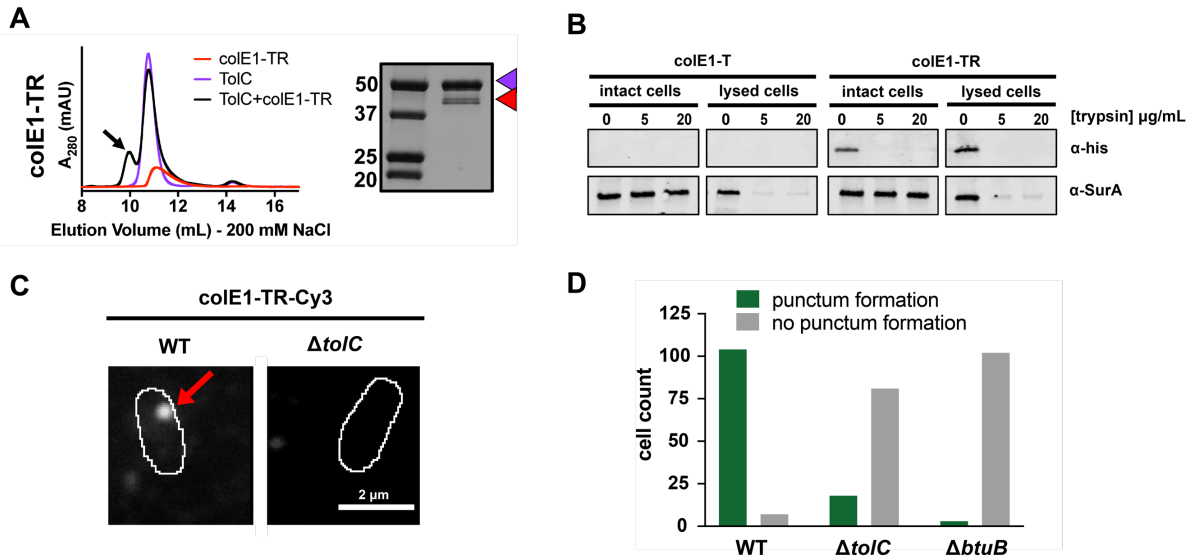

Figure 4. Colicin E1-TR localizes on the outside of the cell. (**A**) SEC chromatogram of colE1-TR (red line) and TolC (purple line). The arrow indicates the co-elution (black line) fractions that were analyzed by SDS-PAGE. On the SDS-PAGE gels (right), red arrow indicates the presence of colicin E1 construct that has co-eluted with TolC (purple arrow). (**B**) Extracellular protease digestion assay with two colicin E1 truncation constructs, each labeled with a C-terminal His-Tag. Periplasmic SurA was used as a membrane integrity control. (**C**) Fluorescence image of colE1-TR-Cy3 overlaid on outlines of living *E. coli* cells from phase-contrast microscopy for WT and Δ*tolC*. Red arrow points to a punctum. (**D**) Cell counts where colE1-TR-Cy3 punctum formation was observed for WT, Δ*tolC*, and Δ*btuB*. Number of cells observed, n = 111, 91, 105, respectively.

241 used to detect translocation across the outer membrane of *Pseudomonas aeruginosa*(*46*). Here we

242 use an analogous experiment with fluorescently labeled colE1 to determine cellular localization in

243 *E. coli*. In time courses, bound colE1-TR puncta remained immobile for > 5 minutes (Movie S1
244 corresponds to the first 8 seconds of data used to attain the WT image in Figure 4C). This is
245 consistent with continued association of colE1-TR with membrane-embedded BtuB, which has
246 limited mobility(*47*). This result indicates that colE1-TR does not fully translocate(*46*), because if
247 colE1-TR entered the periplasmic space it would freely diffuse on these timescales.

248 Colicin constructs lacking the R domain (colE1-T-Cy3) showed no detectable binding
249 either to WT or Δ*tolC* cells (Figure S3C), indicating that the TolC-colE1-T interaction is much
250 weaker than the BtuB-colE1-TR interaction.

251 Because we only see one punctum per cell, we anticipate that some BtuB and TolC remain
252 unbound because of the geometric constraints of punctum formation. Though BtuB and TolC
253 need to be in close proximity for colE1 binding to occur, when BtuB clusters together in groups
254 of 12 or more, it may exclude TolC. These cluster geometries would therefore lower the number
255 of full binding sites available for the T and R domains of colicin E1.

256 **ColE1-TR inhibits efflux and makes *E. coli* more susceptible to antibiotics**

257 Since the colicin truncations are stalled on their respective OMP receptors, we
258 investigated if this stalling could disrupt native TolC efflux. Real-time efflux inhibition by colicin
259 E1 fragments was assessed using a live-cell assay with N-(2-naphthyl)-1-naphthylamine (NNN)-
260 dye, which is effluxed by the acridine efflux pump and fluoresces when it is localized inside the
261 cell(*48*). NNN efflux can be turned off by the protonophore CCCP, which neutralizes the proton
262 motive force and allows NNN to accumulate within the cell. Active efflux can then be monitored
263 by the fluorescence decay once proton motive force is reenergized by glucose addition(*48-52*).

264 We assessed the ability of colicin E1 truncations to plug TolC by monitoring real-time
265 NNN efflux. Cells exposed to colE1-$T_{100-143}$ did not show lower real-time efflux than untreated
266 cells (Figure 5A). This observation is notable in light of the fact that, in previous conductance
267 studies, similar peptides were shown to bind TolC(*6, 24*) and to occlude the channel(*6, 23*).

268 Cells exposed to colE1-T showed less decay in final fluorescence than untreated cells,
269 indicating that colE1-T partially inhibits efflux (Figure 5B). Finally, exposure to colE1-TR
270 produced no decrease in fluorescence, showing full inhibition of efflux (Figure 5C).

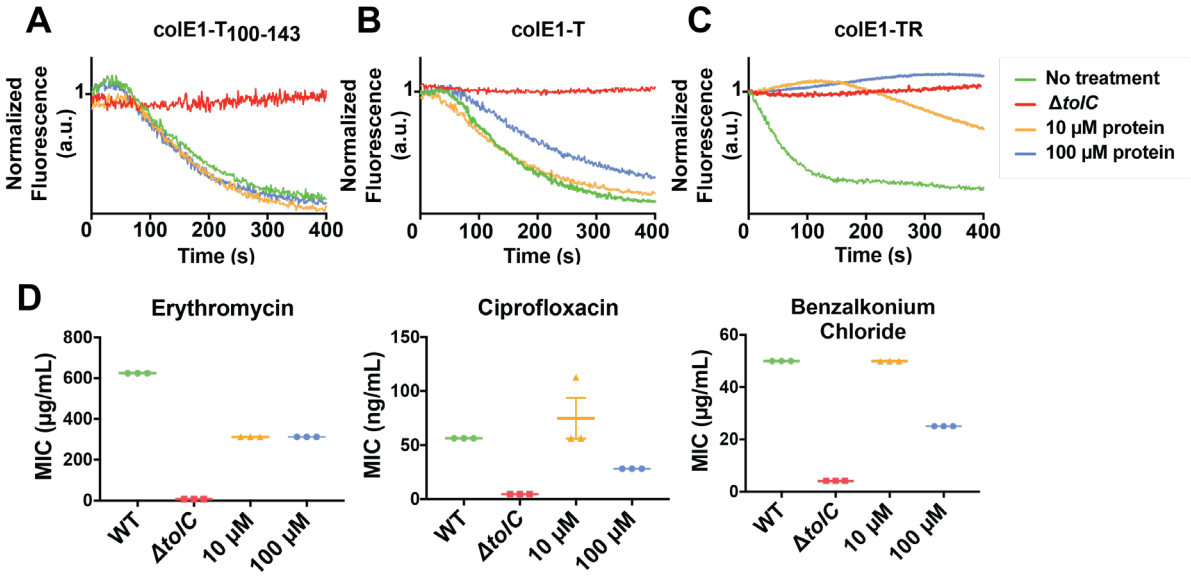

Figure 5. Colicin E1 fragments inhibit efflux and potentiate antibiotics.
(**A-C**) Effect of colicin E1 fragments on efflux: WT with no protein (green), Δ*tolC* (red), WT + 10 μM (orange), WT + 100 μM protein (blue). (**A**) colE1-$T_{100-143}$, (**B**) colE1-T, (**C**) colE1-TR. (**D**) Antibiotic susceptibilities in the absence (green) and presence of colE1-TR added to WT at 10 μM (orange) and 100 μM (blue). MICs for Δ*tolC* (red) are included as a reference. Data are biological replicates reported as the mean and individual data points.

271 Because colE1-TR completely inhibits NNN efflux, we evaluated the capacity of colE1-
272 TR to potentiate antibiotics representing three different classes that are known TolC substrates:
273 ciprofloxacin, erythromycin, and benzalkonium chloride (from fluoroquinolones, macrolides, and
274 quaternary ammonium compounds, respectively). An effective TolC plug will reduce the
275 concentration required to inhibit growth as antibiotics remain trapped within the cell. WT *E. coli*
276 cells that were exposed to 100 μM colE1-TR with each of these antibiotics showed significantly
277 lower minimum inhibitory concentrations (MICs), the lowest concentration of antibiotic that
278 inhibits visible growth, than cells exposed to the antibiotics alone (Figure 5D): exposure to 100
279 μM colE1-TR made WT *E. coli* ~2 to 7-fold more susceptible to these antibiotics (Table S2).
280 Exposure of WT cells to 10μM colE1-TR was sufficient to potentiate erythromycin. Engagement

281 of TolA by the N-terminal TolA box of colicin E9 has previously been shown to cause outer
282 membrane defects(*53*) which would lead to enhanced antibiotic susceptibility. To rule out outer
283 membrane-mediated defects caused by the TolA box in colE1, we created a truncation of colE1-
284 TR (colE1-TR$_{\Delta 1\text{-}40}$) lacking the N-terminal 40 residues including the TolA box. The MIC of
285 colE1-TR and colE1-TR$_{\Delta 1\text{-}40}$ are identical (Figure S4) indicating that colE1-TR engagement of
286 TolA does not contribute to the observed antibiotic susceptibility.
287
288 **Discussion**
289
290 There are two conflicting models of colE1 translocation: 1) the total thread model in
291 which the entire colicin unfolds and threads through TolC(*24, 54*) and 2) the pillar model, in
292 which colicin E1 inserts into TolC as a helical hairpin, facilitating LPS-mediated self-
293 translocation of the colicin cytotoxic domain(*6*). Our data support aspects of both models. The
294 belief in a closed hinge conformation of bound colE1 prompted two arguments against the total
295 thread mechanism: 1) the colE1-T closed hinge conformation is too wide to fit through TolC and
296 2) both ends would face the extracellular milieu(*6, 54*). The unanticipated colE1-T hinge opening
297 in the bound state resolves these objections: colicin threads into the TolC barrel with the amino
298 terminus pointing into the periplasm, as the total thread model hypothesized. However, our
299 trypsin digests and single-molecule fluorescence images show colE1-TR stalls at the outer
300 membrane. Though we cannot exclude the possibility that full length protein translocation
301 depends on the C domain, we observe—as hypothesized by the pillar model—that colicin sits
302 inside TolC but does not translocate. However, the architecture of the complex differs from that
303 hypothesized by the pillar model. These results are in agreement with early studies of pore-
304 forming colicins in which trypsin added to the extracellular environment can reverse colicin
305 activity. Digestibility by trypsin, as well as the ability of colE1-T/TolC to reconstitute a
306 monodisperse stable complex *in vitro* are consistent with the colicin remain in in contact with its
307 outer membrane receptors while the cytotoxic domain depolarizes the inner membrane.

308 In addition to demonstrating a colicin insertion mechanism, our observations form the
309 basis of a means to manipulate bacterial import and efflux. Though colicin E1 confers some level
310 of antibiotic potentiation, the relatively high concentration of colE1-TR needed to inhibit efflux
311 may be explained by a combination of the geometric constraints of creating large clusters of BtuB
312 and TolC, low colE1-T-TolC affinity(*55*), and residually unblocked pore, even in the bound state.
313 Because of their limited potency, our colE1-T and colE1-TR fragments are not likely to be
314 practical in direct applications of antibiotic potentiation. However, our proof-of-concept findings
315 offer a potential roadmap for further development. A more potent TolC binder would not need the
316 R domain anchor for affinity. Such a binder could be designed using the atomic details of the
317 colE1-T-TolC structure as a basis. Moreover, this scaffold can be used for efflux pump inhibitors
318 for at least five other bacterial organisms. Each of these organisms has a structurally characterized
319 outer membrane efflux pump that is homologous and structurally similar to TolC(*56*).
320 More broadly, there are at least nine known outer membrane protein receptors for
321 bacteriocins. These outer membrane proteins have a variety of functions including adhesion, iron
322 transport, and general import(*12, 57*). Using this same strategy with fragments derived from other
323 bacteriocins may additionally allow for controlled inhibition of other bacterial functions.
324
325 **Materials and Methods**
326
327 ***E. coli* strains.** *E. coli* strains BW25113 and JW5503-1 were purchased from the Coli Genetic
328 Stock Center (CGSC). JW5503-1 is a tolC732(del)::kan from the parent strain BW25113.
329 BL21(DE3) were used for expression of the colicin constructs and TolC. BL21(DE3) has a
330 premature stop codon at residue 58 of the *btuB* gene and therefore we used it as a Δ*btuB* strain for
331 microscopy.
332 **Expression and Purification**. The gene for colE1-TR was synthesized as a gBlock (Integrated
333 DNA Technologies) and cloned into pET303. Inverse PCR was used to delete the R domain and

334 produce colicin E1-T. The gene for colicin E1-TR-GFP was produced by inserting GFP at the C
335 terminus of colE1-TR.
336 Plasmids were transformed into *E. coli* BL21(DE3) cells and plated on LB + agar + 100 µg/mL
337 carbenicillin. Single colonies were inoculated into 50 mL LB broth with 100 µg/mL carbenicillin
338 and grown overnight at 37 °C with shaking at 250 r.p.m. Proteins were expressed by inoculating
339 1L of TB supplemented with 0.4% glycerol, 10 mM $MgCl_2$ and 100 µg/mL carbenicillin with 20
340 mL of the overnight culture. The culture was grown at 37 °C to an OD600 of 2.0 and induced
341 with 1 mM IPTG. Expression cultures were then grown at 15 °C for 24 hours and harvested at
342 4,000 g for 30 minutes at 4 °C. Cell pellets were resuspended at 3 mL/g of cell pellet in lysis
343 buffer (TBS, 5 mM $MgCl_2$, 10 mM imidazole, 1mM PMSF, 10 µg/mL DNase, 0.25 mg/mL
344 lysozyme) and lysed via sonication (2 minutes, 2s on, 8s off, 40% amplitude, QSonica Q500 with
345 12.7 mm probe) in an ice bath. Lysates were centrifuged at 4,000 g for 10 minutes to remove un-
346 lysed cells and debris. The supernatant was centrifuged again at 50,400 g in a Beckman Coulter
347 J2-21 for 1 hour at 4 °C. Clarified lysates were applied to a 5 mL HisTrap FF column and purified
348 using an ÄKTA FPLC system with a 20 column volume wash step with binding buffer (TBS, 25
349 mM imidazole) and eluted using a linear gradient from 0-50% elution buffer (TBS, 500 mM
350 imidazole) in 10 column volumes. Concentrated proteins were loaded onto a HiLoad Superdex
351 16/60 200 pg gel filtration column and eluted into phosphate buffered saline (PBS) pH 7.4.
352 TolC expression and purification was conducted in the same manner for preparation for cryoEM
353 and for SEC. The gene for full-length TolC (a generous gift from R. Misra) was cloned into
354 pTrc99a with the signal sequence deleted for expression into inclusion bodies. Plasmids were
355 transformed into BL21(DE3) and plated on LB + agar + 100 µg/mL carbenicillin. A single colony
356 was picked and grown in LB at 37 °C with shaking at 250 r.p.m. overnight. In the morning, 1L of
357 LB was inoculated with 20 mL of the overnight culture and grown at 37 °C with shaking at 250
358 r.p.m. until the culture reached an OD600 of 0.6, at which point protein expression was induced

359 with 1mM IPTG for an additional 4 hours. Cells were then harvested at 4,000g for 30 minutes at 4
360 °C. Cell pellets were resuspended in mL of lysis buffer (TBS, 5 mM $MgCl_2$, 0.2 mg/mL
361 lysozyme, 5 µg/mL DNase, 1mM PMSF) at 3 mL/1g of cell pellet and lysed via sonication (4
362 minutes, 2s on, 8s off, 40% amplitude, QSonica Q500 with 12.7 mm probe) in an ice bath. Cell
363 lysates were centrifuged at 4,000 g for 30 minutes at 4 °C to harvest inclusion bodies. Inclusion
364 body pellets were resuspended in inclusion body wash buffer (20 mM Tris pH 8.0, 0.5 mM
365 EDTA, 1% Triton X-100) and centrifuged at 4,000g for 30 minutes at 4 °C. The inclusion body
366 wash was repeated two more times. A final wash was done in 20 mM Tris pH 8.0 and inclusion
367 bodies were stored at -20 °C. Inclusion bodies were solubilized in 20 mM Tris pH 8.0, 8M urea at
368 500 µM. N-octylpolyoxyethylene was added to 5 mL of solubilized TolC to a final concentration
369 of 10% detergent and pipetted into a Slide-A-Lyzer G2 dialysis cassette with a 10,000 molecular
370 weight cut off. Refolding was initiated by dialysis in 5L of 20 mM Tris pH 8.0, 100 mM NaCl at
371 4 °C with stirring overnight. TolC was centrifuged at 15,200 g for 10 minutes at 4 °C to remove
372 aggregates. The supernatant was filtered through a 0.22 µm filter, concentrated to 2 mL, applied
373 onto a HiLoad 16/60 Superdex 200 pg column on an ÄKTA Pure FPLC system, and eluted with
374 1.5 column volumes in 20 mM Tris pH 8.0, 100 mM NaCl, 0.05% n-dodecyl-β-D-maltoside.
375 TolC containing fractions were pooled and concentrated to 300 µM in Amicon centrifugal filters
376 with molecular weight cutoff of 30kDa.
377 Membrane scaffold protein MSP1D1. MSP1D1 in pET28a was purchased from Addgene and was
378 expressed and purified as previously described(*58*).
379 **Peptide Synthesis.** ColE1-T100-143 was synthesized using standard Fmoc chemistry with a
380 CEM liberty blue microwave peptide synthesizer. The peptides were cleaved using a solution of
381 92.5:2.5:2.5:2.5 TFA:TIPS:H2O:DoDt and the crude peptides where purified using HPLC.
382 Analytical HPLC traces were acquired using an Agilent 1100 quaternary pump and a Hamilton
383 PRP-1 (polystyrene-divinylbenzene) reverse phase analytical column (7 µm particle size, 4 mm x

384 25 cm) with UV detection at 215 nm. The eluents were heated to 45 °C to reduce separation of
385 rotational isomers, and elution was achieved with gradients of water/ acetonitrile (90:10 to 0:100
386 containing 0.1% TFA) over 20 min. Low-resolution mass spectra (LRMS) were obtained using a
387 Waters Micromass ZQ 4000 instrument with ESI+ ionization

388 **Extracellular Protease Digestion.** Protein localization after exogenous protein addition to whole
389 cells was determined as previously described (*39*) with one modification. Samples for intact cells
390 were lysed prior to loading on SDS-PAGE by adding 0.2 mg/mL lysozyme and incubating for 15
391 minutes followed by five freeze thaw cycles in liquid nitrogen.

392 **Single-Molecule Microscopy.** Cysteine mutations were introduced at the C-terminus before the
393 histidine tag for fluorophore conjugation. These constructs were purified as described in the
394 expression and purification section with the addition of 1 mM TCEP in all buffers. All subsequent
395 steps were performed with limited exposure to light and in amber tubes. Cyanine3 (Cy3)
396 maleimide (Lumiprobe) was reconstituted in DMSO. Fluorophore labeling was achieved by
397 mixing a 20-fold molar excess of Cy3 maleimide to protein and incubating overnight at 4 °C. Free
398 dye was removed by gel filtration on a Sephadex NAP-10 G-25 column. Simultaneously to the
399 dye removal, the sample was buffer exchanged into storage buffer (PBS pH 7.4, 1 mM DTT, 1
400 mM EDTA). The degree of labeling was determined spectrophotometrically from the
401 concentrations of the dye and protein solutions using their respective extinction coefficients, ε, as
402 described by their manufacturers or for the proteins as estimated by Expasy ProtParam (Cy3
403 ε548nm = 162,000 L mol-1 cm-1; colE1-T-E192C ε280nm = 9,970 L mol-1 cm-1; colE1-TR-
404 E366C ε280nm = 14,440 L mol-1 cm-1). Labeling efficiencies were ~75% and ~85% for colE1-
405 T-E192C and colE1-TR-E366C, respectively. Protein concentrations were adjusted according to
406 the percentage of labeled protein.

407 Cultures of *E. coli* (WT, ΔtolC, or BL21(DE3)) were grown in LB medium at 37 °C with shaking
408 (180 r.p.m.) overnight, then transferred to MOPS minimal medium (Teknova) with 0.2% glycerol

409 and 1.32 mM K_2HPO_4, and grown at 37 °C for 13 h. The sample was transferred to MOPS
410 medium and grown to turbidity at 37 °C overnight. A 1-mL aliquot of culture was centrifuged for
411 2 min at 4,850 g to pellet the cells. The pellet was washed in 1 mL MOPS and centrifuged a
412 second time. The supernatant was then removed, and the cell pellet was resuspended in 500 µL
413 MOPS. A 1.0 µL droplet of concentrated cells was placed onto a glass slide. Then, a 1.0 µL
414 droplet of 1 µg/mL colicin E1 protein construct stock was added to the cells. The droplet was
415 covered by an agarose pad (1% agarose in MOPS media) and a second coverslip.
416 Samples were imaged at room temperature using wide-field epifluorescence microscopy with
417 sensitivity to detect single dye molecules as described previously (*40*). Briefly, fluorescence was
418 excited by a 561-nm laser (Coherent Sapphire 560-50) for Cy3 or a 488-nm laser (Coherent
419 Sapphire 488-50) for GFP. The lasers were operated at low power densities (1 – 2 W/cm2), and
420 fluorescence was imaged with an Olympus IX71 inverted microscope with a 100x, 1.40-NA
421 phase-contrast oil-immersion objective and appropriate excitation, emission, and dichroic filters.
422 A Photometrics Evolve electron multiplying charge-coupled device (EMCCD) camera with >
423 90% quantum efficiency captured the images at a rate of 20 frames per second. Each detector
424 pixel corresponds to a 49 nm × 49 nm area of the sample. Phase-contrast images of cells were
425 segmented to attain *E. coli* cell outlines using a custom MATLAB script (The MathWorks,
426 Natick, MA).
427 **Co-elution.** The interaction of TolC and colicin E1-T or -TR were determined by co-elution on an
428 SEC column. Purified TolC and colicin E1-T or -TR were mixed at a 1:2 molar ratio to ensure an
429 excess of colicin to saturate TolC binding sites and incubated at room temperature for 1 hour
430 before loading onto a Superdex 200 Increase 10/300 GL column (GE Healthcare). The protein
431 was eluted with 1.5 column volumes into 20 mM Tris pH 8.0, 40 mM NaCl, 0.05% n-dodecyl-β-
432 D-maltoside for colE1-T. For colE1-TR the NaCl concentration was increased to 200 mM to

433 prevent precipitation. Elution fractions were collected every 0.5 mL. Peak fractions were
434 concentrated to 20 µL and analyzed by 4-20% SDS-PAGE.
435 **Real-Time Efflux.** Real-time efflux activity in the presence of colE1-TR was determined as
436 previously described with some modifications(*48, 49*). Cells were resuspended to OD600 1.5 in
437 cold PBS with and without 10-100 µM colicin proteins and incubated for 15 minutes on ice. To
438 turn off efflux, 100µM carbonyl cyanide m-chlorophenyl hydrazone (CCCP) was added. After an
439 additional 15 minutes the efflux dye NNN was added to the cells to 10 µM. The cells were
440 incubated at 25 °C with shaking at 140 r.p.m. for 2 hours. Cells were harvested at 3,500 g for 5
441 minutes and washed once in 20 mM potassium phosphate buffer pH 7 with 1mM $MgCl_2$. Cell
442 concentrations were adjusted to OD600 1.0 and placed on ice. Then, 2 mL of the cell suspension
443 was loaded into a quartz cuvette (Agilent Technologies). Fluorescence was measured with an
444 Agilent Cary Eclipse fluorescence spectrophotometer with slit widths at 5 and 10 nm for
445 excitation wavelength of 370 nm and emission wavelength of 415 nm. Fluorescence
446 measurements were taken every 1 second. After 100 seconds, 50 mM glucose was added to re-
447 energize the cells and initiate efflux, and fluorescence data were collected for an additional 600
448 seconds. Figure 5A-C, reflects time after glucose addition.
449
450 **Minimum Inhibitory Concentrations (MICs).** MICs were determined using the broth dilution
451 method(*59*) with some modifications in 96 well plate format using LB media in 100 µL well
452 volumes. Cultures were grown at 37 °C with shaking at 250 r.p.m. and OD600 was read on a
453 Biotek plate reader after 20 hours. MICs are defined by the lowest concentration that prevents
454 visible growth. We chose an OD600 of >0.1 as the cutoff for growth. We report MICs as the
455 mean of 3 or 6 biological replicates with each replicate plotted (Figure 3D, Table S2). Due to the
456 2-fold discretized nature of concentration ranges used to determine MICs we do not report
457 statistical significance values as is typical of MIC reporting.

458 **Reconstitution of TolC into Amphipol.** Amphipol A8-35 (Anatrace) was solubilized in water at
459 33 mgs/mL. 1 mL of TolC at 0.5 mg/mL was mixed with 0.75 µL of A8-35 at 33 mg/mL for a 5-
460 fold weight excess and incubated at room temperature for 30 minutes. Bio-Beads SM-2 resin that
461 was washed in methanol and equilibrated with 20 mM Tris, 40 mM NaCl was added to the
462 reaction mixture at 0.5 g/mL to initiate detergent exchange for A8-35 and incubated with rotation
463 at 4 °C overnight. The mixture was transferred to a tube with fresh Bio-Beads and incubated at 4
464 °C for an additional 4 hours. The reaction mixture was loaded onto a HiLoad 16/60 Superdex 200
465 pg column on an ÄKTA Pure FPLC system and eluted with 1.5 column volumes in 20 mM Tris
466 pH 8.0, 40 mM NaCl to remove free A8-35 and detergent. For colicin-bound TolC in A8-35,
467 colicin E1-T was added to the reaction mixture at a >2 molar excess prior to gel filtration. TolC or
468 colicin-bound TolC in A8-35 was concentrated to 2-4 mg/mL for cryoEM.
469 **Reconstitution of TolC into lipid nanodiscs.** POPC (Avanti Polar Lipids) in chloroform was
470 dried under a stream of nitrogen and freeze dried to remove residual chloroform. Lipids were
471 reconstituted to 50 mM in cholate buffer (20 mM Tris pH 8.0, 100 mM NaCl, 0.5 mM EDTA,
472 100 mM cholate) in an amber glass vial. The vial was submerged under a stream of warm water
473 until the solution became clear. Lipids, membrane scaffold protein, and TolC were mixed in a
474 36:1:0.4 ratio as previously described(*60*). Final concentrations were 4.5 mM POPC, 125 µM
475 MSP1D1, 50 µM TolC in a 2 mL reaction with cholate brought up to 20 mM and dodecyl-
476 maltoside up to 0.1%. The reaction mixture was incubated on ice for 1 hour. Bio-Beads SM-2
477 resin that was washed in methanol and equilibrated with 20 mM Tris, 40 mM NaCl were added to
478 the reaction mixture at 0.5 g/mL to initiate nanodisc formation and incubated with rotation at 4°C
479 overnight. The mixture was transferred to a tube with fresh Bio-Beads and incubated at 4 °C for
480 an additional 4 hours. The reaction mixture was loaded onto a HiLoad 16/60 Superdex 200 pg
481 column on an ÄKTA Pure FPLC system and eluted with 1.5 column volumes in 20 mM Tris pH
482 8.0, 40 mM NaCl to separate TolC inserted into nanodiscs from empty nanodiscs. For colicin-

483 bound TolC in nanodiscs, colicin E1-T was added to the reaction mixture at a >2 molar excess
484 prior to gel filtration. TolC or colicin-bound TolC in nanodiscs was concentrated to 2-4 mg/mL
485 for cryoEM.
486 **Cryoelectron microscopy.** 3 μL of protein solution (TolC/colE1-T in amphipol or TolC/colE1-T
487 in nanodiscs) was diluted to approximately 1.05 mg/mL concentration, applied to a glow-
488 discharged TEM grid, and plunge-frozen in ethane using a Vitrobot Mark IV (FEI Company) with
489 grade 595 filter paper (Ted Pella). Glow discharge was performed in ambient atmosphere at 0.39
490 mBar pressure. Imaging was performed using a Talos Arctica (FEI Company) operated at 200 kV
491 with energy-filter and K2 Summit (Gatan, Inc.) for detection. To collect multiple images per hole
492 while maintaining parallel illumination conditions, a nonstandard 20 μm condenser aperture was
493 used to image TolC-colE1-T in nanodiscs. At nominal magnification of 205,000×, images were
494 acquired in counting mode with a calibrated pixel size of 0.6578 Å. Fresnel fringes attributable to
495 the beam interaction with the aperture were often seen in images. Some investigators have moved
496 the microscope stage and altered the nominal objective lens true focus point to generate a fringe-
497 free condition(*61*). In this study, imaging at 205,000× with a 20 μm aperture yielded better results
498 than imaging at 130,000× with a 50 μm aperture; at 130,000× with a 20 μm aperture the fringes
499 were extremely severe due to the larger field of view, so a full dataset was not collected with
500 those conditions. TolC in nanodiscs (without colE1-T) was imaged at 130,000× with a 50μm
501 condenser aperture (Table S1).
502 Micrographs were collected with SerialEM(*62*) using in-house modifications of the scripts of
503 Chen Xu (sphinx-emdocs.readthedocs.io). Briefly, multishot imaging was configured with 4
504 images per hole for each of 16 holes; intermediate-magnification montages of grid squares were
505 acquired; points were selected manually for collection of 64 images per point; images were
506 acquired using coma-compensated image shift as gain- and dark-corrected LZW-compressed

507 TIFs. Side, top, and oblique views were seen in areas of thin ice. During screening, ice thickness
508 was estimated at 17-30nm by the method of I_0/I_{ZLP}(*63*).
509 The collection of micrographs of TolC without colicin at 130,000× magnification has been
510 previously described(*64*).
511 **3D reconstruction and modeling.** Final reconstructions were obtained using cryoSPARC 2(*65*).
512 1,018 micrographs were collected of amphipol-embedded TolC/colE1-T. Micrographs were
513 motion-corrected using RELION 3(*66*). CTF parameters were determined by means of
514 *ctffind*(*67*). 115,362 particles were selected with crYOLO(*68*). 2D classification revealed that
515 many particles had aberrant morphology and only 24,624 (21%) were selected for 3D
516 reconstruction. *Ab initio* reconstruction in cryoSPARC 2(*65*) was effective at recovering a map
517 whose shape was similar to that of previously described TolC trimers. However, the data could
518 only be refined to a nominal global resolution of 6.0 Å, and lumenal density was insufficiently
519 resolved. 4,492 micrographs were then collected of nanodisc-embedded TolC/colE1-T and
520 processed similarly. Of the 339,779 particles detected by cryoSPARC Live, 179,834 (53%) were
521 in good classes. Although there were slightly fewer particles per micrograph in the nanodisc
522 dataset, more particles per micrograph were usable. Beginning with the *ab initio* model and mask
523 derived from the amphipol data, this particle set was refined by cryoSPARC 2 non-uniform
524 refinement with or without imposed C_3 symmetry. The maps refined to nominal global resolutions
525 of 2.81 Å and 3.09 Å for the symmetrized and asymmetric maps, respectively. There was local
526 variation in resolution within the map, with consistent, high resolution in the middle of TolC and
527 lower resolution at the lids and for colE1-T. Local resolution was computed in cryoSPARC by the
528 locally windowed FSC method(*69*) and rendered with UCSF Chimera. To reduce the voxel-based
529 values to averages for four regions of the complex, the local resolution map was masked to
530 include only voxels within 3 Å of a modeled atom and then the median value was calculated for
531 those voxels closest to colE1, closest to TolC residues 168-172 and 386-390, closest to TolC

532 residues 285-301 and 76-82, or closest to other TolC residues. Furthermore, it is notable that
533 while the nanodisc appears as a double-belt in the symmetrized map, in the asymmetric map the
534 nanodisc protein mostly appears on the side of TolC that is bound to colE1-T. One possible
535 explanation is that, despite masking, nanodisc asymmetry is a confounder of the asymmetric
536 refinement and is one source of heterogeneity in the data. Another possibility is that the C-
537 terminus of colE1-T forms an interaction with the nanodisc, causing preferential alignment of the
538 nanodisc with respect to the TolC/colE1-T complex.
539 196,158 particles of TolC without colicin were obtained as previously described(*64*).
540 Homogeneous refinement yielded a structure at 2.89 Å; local motion correction and global CTF
541 refinement yielded a final map at 2.84 Å.
542 Modeling was initiated by rigidly docking a crystal structure of TolC in complex with
543 hexamminecobalt (1TQQ)(*31*) into the symmetrized map density. Automated, semi-automated,
544 and manual real-space refinement was performed using phenix(*70*), ISOLDE(*71*), and coot(*72*).
545 For TolC with colE1-T, additional refinement was performed in AMBER using the cryoEM
546 density map as a restraint.
547 Although additional residues are present at the TolC C-terminus, these were not modeled because
548 the density becomes unsharp after residue 428. Blurred density in the map suggests that the C-
549 terminus follows helix 3 towards the periplasmic end of the molecule. ColE1-T was modeled *ab*
550 *initio*. The 3-fold symmetrized map contains density at ~1/3rd occupancy for colE1-T and this
551 density contains some high-resolution information not present in the asymmetric map, except near
552 the TolC lid regions where symmetrization overlays colE1-T density with TolC density at a
553 threefold-related position. First, polyalanine helices were placed in the helical density in coot.
554 Cross-correlation coefficients for both helices are higher with the N-terminus oriented towards the
555 periplasm, and the Christmas tree appearance was observed indicating that this is the correct chain
556 orientation. An estimate of the registration was made by visual inspection of potential anchor

557 residues. Finally, the hinge region was filled in using phenix and coot. This completed chain was
558 refined against the asymmetric map in ISOLDE. Iteration between phenix, coot, and ISOLDE was
559 continued until acceptable fit to density was achieved. In the case of TolC with colE1-T, the map
560 was further improved by combining map information with molecular dynamics force fields(*34*).
561 Briefly, starting with the phenix/coot/ISOLDE-refined model, we performed restrained simulated
562 annealing in AMBER, heating from 0K to 300K for 0.2 nsec, holding constant temperature for 1
563 nsec, and then cooling to 0K over 0.2 nsec. The cryoEM density map is utilized as a restraint
564 potential in the annealing so that both map information and AMBER force field information are
565 simultaneously utilized to obtain an optimum model consistent with the data(*34*). The protein
566 force field used the ff14SB force field(*73*) and a generalized Born implicit solvent model with
567 *igb=8*(*74*), and a nonbonded cutoff of 20 Å. The relative weight of real-space map-based
568 restraints and the force field was fixed using *fcons=0.02*. For colE1-T, information from the
569 symmetrized map was integrated into the modeling procedure during manual remodeling in coot,
570 but map-based refinement in phenix, ISOLDE, and AMBER were against the asymmetric map.
571 TolC without colE1-T was modeled similarly but using the TolC-colE1-T structure as a starting
572 point instead of 1TQQ, and without final AMBER refinement.
573 Molecular representations were generated with Chimera, ChimeraX(*75*) or PyMOL (Schrödinger,
574 LLC).
575
576 **References**
577
578 1. T. Kawabata, Detection of multiscale pockets on protein surfaces using mathematical
579 morphology. *Proteins* **78**, 1195-1211 (2010).
580 2. T. Kawabata, Detection of cave pockets in large molecules: Spaces into which internal
581 probes can enter, but external probes from outside cannot. *Biophys Physicobiol* **16**, 391-
582 406 (2019).
583 3. T. Kawabata, N. Go, Detection of pockets on protein surfaces using small and large probe
584 spheres to find putative ligand binding sites. *Proteins* **68**, 516-529 (2007).
585 4. J. Yang *et al.*, The I-TASSER Suite: protein structure and function prediction. *Nat*
586 *Methods* **12**, 7-8 (2015).
587 5. C. Alexander, E. T. Rietschel, Invited review: Bacterial lipopolysaccharides and innate
588 immunity. *Journal of Endotoxin Research* **7**, 167-202 (2001).

589 6. S. D. Zakharov, X. S. Wang, W. A. Cramer, The Colicin E1 TolC-Binding Conformer:
590 Pillar or Pore Function of TolC in Colicin Import? *Biochemistry* **55**, 5084-5094 (2016).
591 7. Y. Kamio, H. Nikaido, Outer membrane of Salmonella typhimurium: accessibility of
592 phospholipid head groups to phospholipase c and cyanogen bromide activated dextran in
593 the external medium. *Biochemistry* **15**, 2561-2570 (1976).
594 8. J. T. C. Freeman, W. C. Wimley, TMBB-DB: a transmembrane β-barrel proteome
595 database. *Bioinformatics* **28**, 2425-2430 (2012).
596 9. W. A. Cramer, O. Sharma, S. D. Zakharov, On mechanisms of colicin import: the outer
597 membrane quandary. *Biochem J* **475**, 3903-3915 (2018).
598 10. S. K. Buchanan *et al.*, Structure of colicin I receptor bound to the R-domain of colicin Ia:
599 implications for protein import. *EMBO J* **26**, 2594-2604 (2007).
600 11. G. Kurisu *et al.*, The structure of BtuB with bound colicin E3 R-domain implies a
601 translocon. *Nat Struct Biol* **10**, 948-954 (2003).
602 12. E. Cascales *et al.*, Colicin Biology. *Microbiology and Molecular Biology Reviews* **71**, 158-
603 229 (2007).
604 13. N. G. Housden *et al.*, Directed epitope delivery across the Escherichia coli outer
605 membrane through the porin OmpF. *Proc Natl Acad Sci U S A* **107**, 21412-21417 (2010).
606 14. O. Sharma *et al.*, Structure of the complex of the colicin E2 R-domain and its BtuB
607 receptor. The outer membrane colicin translocon. *J Biol Chem* **282**, 23163-23170 (2007).
608 15. H. Benedetti *et al.*, Individual domains of colicins confer specificity in colicin uptake, in
609 pore-properties and in immunity requirement. *J Mol Biol* **217**, 429-439 (1991).
610 16. H. Benedetti *et al.*, Comparison of the Uptake Systems for the Entry of Various BtuB
611 Group Colicins into Escherichia coli. *Microbiology* **135**, 3413-3420 (1989).
612 17. P. Elkins, A. Bunker, W. A. Cramer, C. V. Stauffacher, A mechanism for toxin insertion
613 into membranes is suggested by the crystal structure of the channel-forming domain of
614 colicin E1. *Structure* **5**, 443-458 (1997).
615 18. C. A. Plate, S. E. Luria, Stages in colicin K action, as revealed by the action of trypsin.
616 *Proc Natl Acad Sci U S A* **69**, 2030-2034 (1972).
617 19. J. Dankert, S. M. Hammond, W. A. Cramer, Reversal by trypsin of the inhibition of active
618 transport by colicin E1. *J Bacteriol* **143**, 594-602 (1980).
619 20. J. R. Dankert, Y. Uratani, C. Grabau, W. A. Cramer, M. Hermodson, On a domain
620 structure of colicin E1. A COOH-terminal peptide fragment active in membrane
621 depolarization. *J Biol Chem* **257**, 3857-3863 (1982).
622 21. H. Benedetti, R. Lloubes, C. Lazdunski, L. Letellier, Colicin A unfolds during its
623 translocation in Escherichia coli cells and spans the whole cell envelope when its pore has
624 formed. *EMBO J* **11**, 441-447 (1992).
625 22. S. D. Zakharov, X. S. Wang, W. A. Cramer, The Colicin E1 TolC-Binding Conformer:
626 Pillar or Pore Function of TolC in Colicin Import? *Biochemistry* **55**, 5084-5094 (2016).
627 23. S. D. Zakharov *et al.*, Colicin occlusion of OmpF and TolC channels: outer membrane
628 translocons for colicin import. *Biophys J* **87**, 3901-3911 (2004).
629 24. K. S. Jakes, The Colicin E1 TolC Box: Identification of a Domain Required for Colicin E1
630 Cytotoxicity and TolC Binding. *J Bacteriol* **199**, (2017).
631 25. M. Wiener, D. Freymann, P. Ghosh, R. M. Stroud, Crystal structure of colicin Ia. *Nature*
632 **385**, 461-464 (1997).
633 26. N. G. Housden *et al.*, Intrinsically disordered protein threads through the bacterial outer-
634 membrane porin OmpF. *Science* **340**, 1570-1574 (2013).
635 27. A preprint of this work was first published on *bioRxiv* (692251) in July 2019 and updated
636 with the structure May 2021.
637 28. K. M. Storek *et al.*, Monoclonal antibody targeting the beta-barrel assembly machine of
638 Escherichia coli is bactericidal. *Proc Natl Acad Sci U S A* **115**, 3692-3697 (2018).

639 29. S. J. Budiardjo *et al.*, High-Yield Preparation of Outer Membrane Protein Efflux Pumps
640 by in Vitro Refolding is Concentration Dependent. *J Membr Biol* **254**, 41-50 (2021).
641 30. V. Koronakis, A. Sharff, E. Koronakis, B. Luisi, C. Hughes, Crystal structure of the
642 bacterial membrane protein TolC central to multidrug efflux and protein export. *Nature*
643 **405**, 914-919 (2000).
644 31. M. K. Higgins *et al.*, Structure of the ligand-blocked periplasmic entrance of the bacterial
645 multidrug efflux protein TolC. *J Mol Biol* **342**, 697-702 (2004).
646 32. N. G. Housden *et al.*, Directional Porin Binding of Intrinsically Disordered Protein
647 Sequences Promotes Colicin Epitope Display in the Bacterial Periplasm. *Biochemistry* **57**,
648 4374-4381 (2018).
649 33. R. Dhar, R. Feehan, J. S. G. Slusky, Membrane Barrels Are Taller, Fatter, Inside-Out
650 Soluble Barrels. *J Phys Chem B* **125**, 3622-3628 (2021).
651 34. X. Wu, S. Subramaniam, D. A. Case, K. W. Wu, B. R. Brooks, Targeted conformational
652 search with map-restrained self-guided Langevin dynamics: application to flexible fitting
653 into electron microscopic density maps. *J Struct Biol* **183**, 429-440 (2013).
654 35. C. J. Williams *et al.*, MolProbity: More and better reference data for improved all-atom
655 structure validation. *Protein Sci* **27**, 293-315 (2018).
656 36. B. A. Barad *et al.*, EMRinger: side chain-directed model and map validation for 3D cryo-
657 electron microscopy. *Nat Methods* **12**, 943-946 (2015).
658 37. M. Masi, P. Vuong, M. Humbard, K. Malone, R. Misra, Initial steps of colicin E1 import
659 across the outer membrane of Escherichia coli. *J Bacteriol* **189**, 2667-2676 (2007).
660 38. K. R. Brunden, Y. Uratani, W. A. Cramer, Dependence of the conformation of a colicin
661 E1 channel-forming peptide on acidic pH and solvent polarity. *The Journal of biological*
662 *chemistry* **259**, 7682-7687 (1984).
663 39. R. N. Besingi, P. L. Clark, Extracellular protease digestion to evaluate membrane protein
664 cell surface localization. *Nat Protoc* **10**, 2074-2080 (2015).
665 40. H. H. Tuson, J. S. Biteen, Unveiling the inner workings of live bacteria using super-
666 resolution microscopy. *Anal Chem* **87**, 42-63 (2015).
667 41. N. Al-Husini *et al.*, BR-Bodies Provide Selectively Permeable Condensates that Stimulate
668 mRNA Decay and Prevent Release of Decay Intermediates. *Mol Cell* **78**, 670-682 e678
669 (2020).
670 42. F. W. Studier, P. Daegelen, R. E. Lenski, S. Maslov, J. F. Kim, Understanding the
671 differences between genome sequences of Escherichia coli B strains REL606 and
672 BL21(DE3) and comparison of the E. coli B and K-12 genomes. *J Mol Biol* **394**, 653-680
673 (2009).
674 43. S. Bakshi, A. Siryaporn, M. Goulian, J. C. Weisshaar, Superresolution imaging of
675 ribosomes and RNA polymerase in live Escherichia coli cells. *Mol Microbiol* **85**, 21-38
676 (2012).
677 44. P. Rassam *et al.*, Supramolecular assemblies underpin turnover of outer membrane
678 proteins in bacteria. *Nature* **523**, 333-336 (2015).
679 45. M. Chavent *et al.*, How nanoscale protein interactions determine the mesoscale dynamic
680 organisation of bacterial outer membrane proteins. *Nat Commun* **9**, 2846 (2018).
681 46. P. White *et al.*, Exploitation of an iron transporter for bacterial protein antibiotic import.
682 *Proc Natl Acad Sci U S A* **114**, 12051-12056 (2017).
683 47. C. Kleanthous, P. Rassam, C. G. Baumann, Protein-protein interactions and the
684 spatiotemporal dynamics of bacterial outer membrane proteins. *Curr Opin Struct Biol* **35**,
685 109-115 (2015).
686 48. J. A. Bohnert, S. Schuster, M. Szymaniak-Vits, W. V. Kern, Determination of real-time
687 efflux phenotypes in Escherichia coli AcrB binding pocket phenylalanine mutants using a
688 1,2'-dinaphthylamine efflux assay. *PLoS One* **6**, e21196 (2011).

689 49. J. A. Bohnert, B. Karamian, H. Nikaido, Optimized Nile Red efflux assay of AcrAB-TolC
690 multidrug efflux system shows competition between substrates. *Antimicrob Agents*
691 *Chemother* **54**, 3770-3775 (2010).
692 50. M. A. Seeger *et al.*, Engineered disulfide bonds support the functional rotation mechanism
693 of multidrug efflux pump AcrB. *Nat Struct Mol Biol* **15**, 199-205 (2008).
694 51. R. Iyer, A. Ferrari, R. Rijnbrand, A. L. Erwin, A fluorescent microplate assay quantifies
695 bacterial efflux and demonstrates two distinct compound binding sites in AcrB.
696 *Antimicrob Agents Chemother* **59**, 2388-2397 (2015).
697 52. R. Misra, K. D. Morrison, H. J. Cho, T. Khuu, Importance of Real-Time Assays To
698 Distinguish Multidrug Efflux Pump-Inhibiting and Outer Membrane-Destabilizing
699 Activities in Escherichia coli. *J Bacteriol* **197**, 2479-2488 (2015).
700 53. P. Rassam *et al.*, Intermembrane crosstalk drives inner-membrane protein organization in
701 Escherichia coli. *Nat Commun* **9**, 1082 (2018).
702 54. W. A. Cramer, O. Sharma, S. D. Zakharov, On mechanisms of colicin import: the outer
703 membrane quandary. *Biochemical Journal* **475**, 3903-3915 (2018).
704 55. R. Taylor, J. W. Burgner, J. Clifton, W. A. Cramer, Purification and characterization of
705 monomeric Escherichia coli vitamin B12 receptor with high affinity for colicin E3. *J Biol*
706 *Chem* **273**, 31113-31118 (1998).
707 56. M. W. Franklin *et al.*, Efflux Pumps Represent Possible Evolutionary Convergence onto
708 the beta-Barrel Fold. *Structure* **26**, 1266-1274.e1262 (2018).
709 57. C. Kleanthous, Swimming against the tide: progress and challenges in our understanding
710 of colicin translocation. *Nat Rev Microbiol* **8**, 843-848 (2010).
711 58. F. Hagn, M. L. Nasr, G. Wagner, Assembly of phospholipid nanodiscs of controlled size
712 for structural studies of membrane proteins by NMR. *Nat Protoc* **13**, 79-98 (2018).
713 59. I. Wiegand, K. Hilpert, R. E. Hancock, Agar and broth dilution methods to determine the
714 minimal inhibitory concentration (MIC) of antimicrobial substances. *Nat Protoc* **3**, 163-
715 175 (2008).
716 60. L. Daury *et al.*, Tripartite assembly of RND multidrug efflux pumps. *Nat Commun* **7**,
717 10731 (2016).
718 61. F. Weis, W. J. H. Hagen, Combining high throughput and high quality for cryo-electron
719 microscopy data collection. *Acta Crystallogr D Struct Biol* **76**, 724-728 (2020).
720 62. D. N. Mastronarde, Advanced Data Acquisition From Electron Microscopes With
721 SerialEM. . *Microscopy and Microanalysis* **24**, 864-865 (2018).
722 63. W. J. Rice *et al.*, Routine determination of ice thickness for cryo-EM grids. *J Struct Biol*
723 **204**, 38-44 (2018).
724 64. S. J. Budiardjo *et al.*, High yield preparation of outer-membrane protein efflux pumps by
725 in vitro refolding is concentration dependent. *bioRxiv*,
726 2020.2009.2014.296756 (2020).
727 65. A. Punjani, J. L. Rubinstein, D. J. Fleet, M. A. Brubaker, cryoSPARC: algorithms for
728 rapid unsupervised cryo-EM structure determination. *Nat Methods* **14**, 290-296 (2017).
729 66. J. Zivanov *et al.*, New tools for automated high-resolution cryo-EM structure
730 determination in RELION-3. *Elife* **7**, (2018).
731 67. A. Rohou, N. Grigorieff, CTFFIND4: Fast and accurate defocus estimation from electron
732 micrographs. *J Struct Biol* **192**, 216-221 (2015).
733 68. T. Wagner *et al.*, SPHIRE-crYOLO is a fast and accurate fully automated particle picker
734 for cryo-EM. *Commun Biol* **2**, 218 (2019).
735 69. G. Cardone, J. B. Heymann, A. C. Steven, One number does not fit all: mapping local
736 variations in resolution in cryo-EM reconstructions. *J Struct Biol* **184**, 226-236 (2013).
737 70. P. V. Afonine *et al.*, Real-space refinement in PHENIX for cryo-EM and crystallography.
738 *Acta Crystallogr D Struct Biol* **74**, 531-544 (2018).

71. T. I. Croll, ISOLDE: a physically realistic environment for model building into low-resolution electron-density maps. *Acta Crystallogr D Struct Biol* **74**, 519-530 (2018).
72. P. Emsley, B. Lohkamp, W. G. Scott, K. Cowtan, Features and development of Coot. *Acta Crystallogr D Biol Crystallogr* **66**, 486-501 (2010).
73. J. A. Maier *et al.*, ff14SB: Improving the Accuracy of Protein Side Chain and Backbone Parameters from ff99SB. *J Chem Theory Comput* **11**, 3696-3713 (2015).
74. H. Nguyen, D. R. Roe, C. Simmerling, Improved Generalized Born Solvent Model Parameters for Protein Simulations. *J Chem Theory Comput* **9**, 2020-2034 (2013).
75. T. D. Goddard *et al.*, UCSF ChimeraX: Meeting modern challenges in visualization and analysis. *Protein Sci* **27**, 14-25 (2018).

Acknowledgments

We gratefully acknowledge Daniel Montezano, Pinakin Sukthankar, Rik Dhar, Dwight Deay, Scott Lovell, Matthias Wolf, Alexander Little, Heather Shinogle, and Sarah Noga for discussions and feedback, Mark Richter for the use of his fluorometer, Rajeev Misra for the pTrc vector containing the TolC gene, Vasileios Petrou for guidance on nanodiscs, Chamani Perera for peptide synthesis, Karen Marom for editorial guidance. We thank the Office of Advanced Research computing (OARC) at Rutgers for high-performance computing resources.

Funding:
NIH award R21-GM128022 to JSB
NIGMS awards DP2GM128201, P20GM113117, P20GM103638 and the Gordon and Betty Moore Inventor Fellowship to JSGS,
NIGMS awards P20 GM103418 and 2K12GM063651 to SJB.

Author contributions:
Conceptualization: SJB, JSGS
Methodology: SJB, JTK, JSGS, JSB
Investigation: SJB, JJS, ALC, API, VKW, EF, DAC, JTK
Writing—original draft: SJB, JSGS
Writing—review & editing: SJB, JSGS, JSB, JTK

Competing interests: Authors declare that they have no competing interests.

Data and materials availability: All data are available in the main text or the supplementary materials." All strains used are commercially available. All plasmids available through Addgene. CryoEM maps and models have been deposited with accession codes EMD-21960, EMD-21959, PDB ID 6WXI, and PDB ID 6WXH. All other data is available in the main text or the supplementary materials.

advances.sciencemag.org/cgi/content/full/sciadv.[ms.no.]/DC1

Supplementary Materials for

Colicin E1 opens its hinge to plug TolC

S. Jimmy Budiardjo, Jacqueline J. Stevens, Anna L. Calkins, Ayotunde P. Ikujuni, Virangika K. Wimalasena, Emre Firlar, David A. Case, Julie S. Biteen, Jason T. Kaelber and Joanna S.G. Slusky*

*Corresponding author. Email: slusky@ku.edu

This PDF file includes:

Figs. S1 to S4
Tables S1 to S2
Movie caption S1

Other Supplementary Materials for this manuscript include the following:
[use this section only if you have movies, audio or data files]
Movie S1

812 **Fig. S1.**

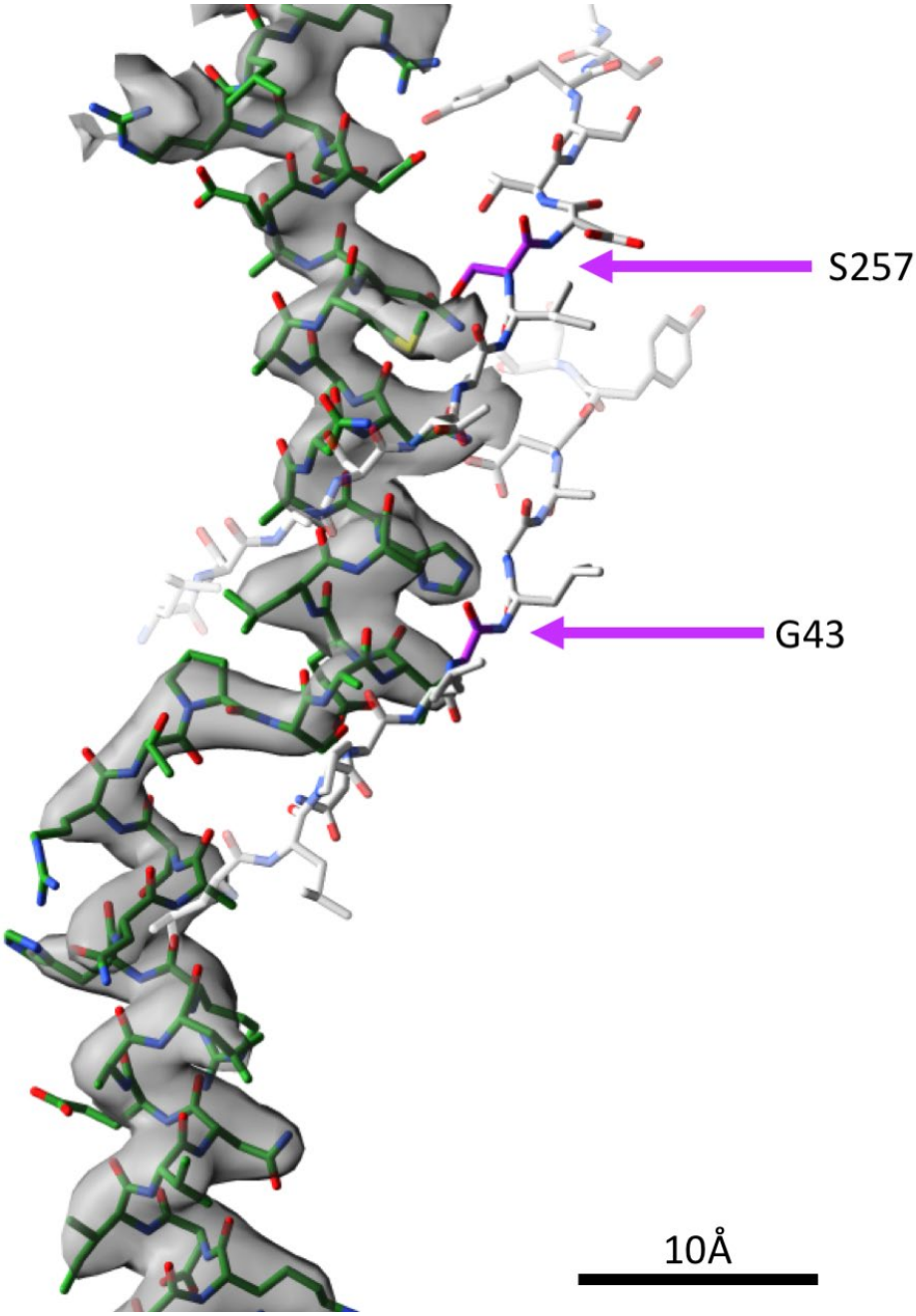

813
814
815 **Figure S1. TolC box density** cropped from the fully asymmetric cryoEM map of the TolC/colE1-T complex.
816 Mutations at positions G43 and S257 in the TolC (grey sticks) barrel make direct contact with colE1-T (green). These
817 mutations were previously shown to abolish WT colE1 function(*37*). Mutations to bulkier side chains introduce a
818 steric clash that prevents binding.
819

820 **Fig. S2.**

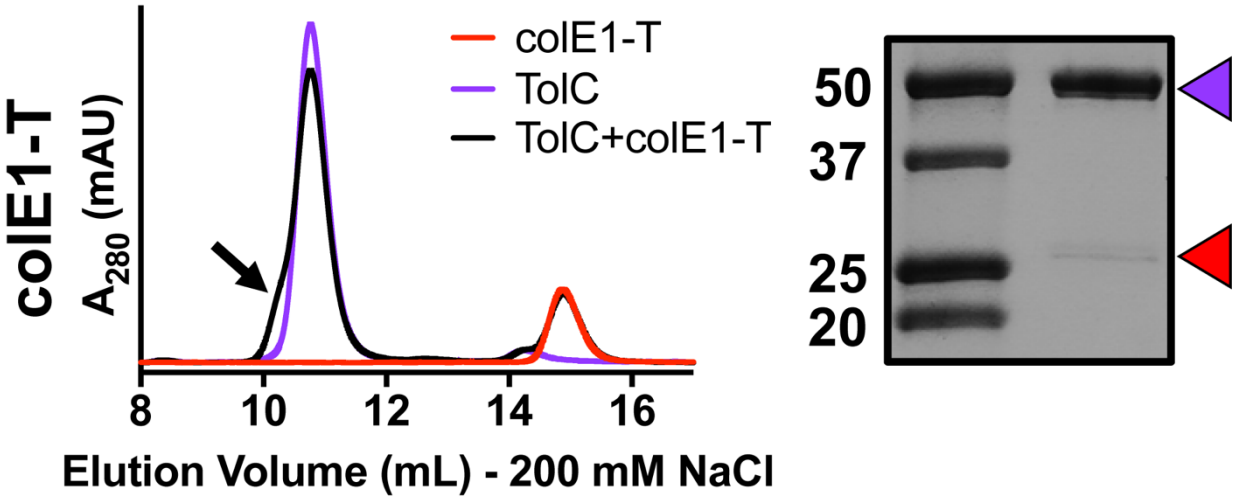

821

822 **Figure S2. Co-elution of colE1-T with TolC at 200 mM NaCl (black).** Under this higher salt
823 concentration, when TolC (purple) and colE1-T (red) are mixed, there is a smaller peak shift than
824 that seen with colE1-TR and the presence of a shoulder (black arrow). SDS-PAGE of the shoulder
825 shows presence of both TolC (purple arrow) and colE1-T (red arrow). Although some binding
826 was detected, this higher salt concentration prevents full binding as indicated by a much fainter
827 band for colE1-T than seen at the lower salt concentration (Figure 4A).

828

829 **Fig. S3.**

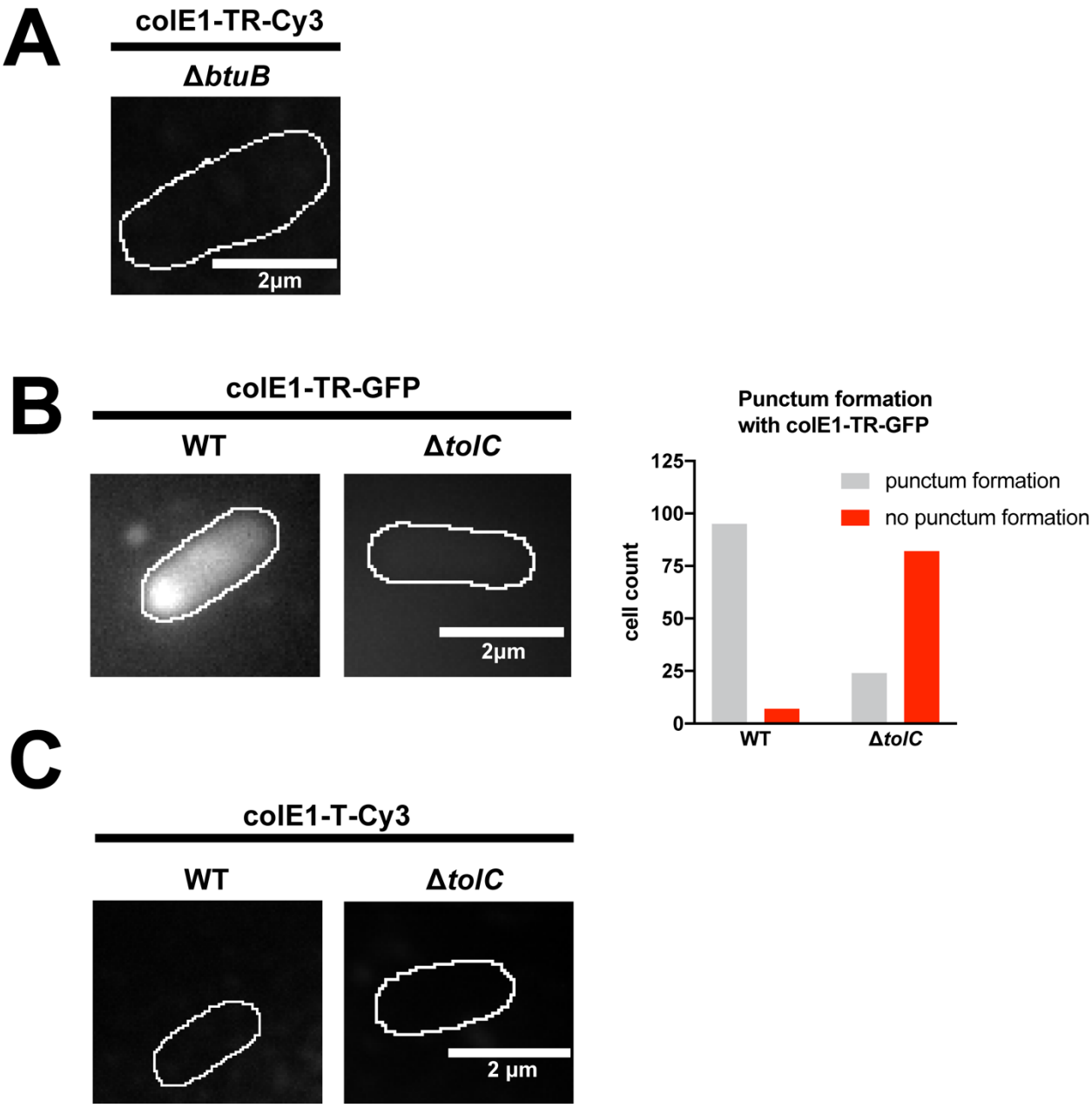

830
831 **Figure S3 Single-molecule microscopy.** Fluorescence images overlaid on outlines of living *E.*
832 *coli* cells from phase-contrast microscopy for WT and Δ*tolC* for colE1-TR-GFP and counts of
833 cells where colE1-TR-GFP punctum formation was observed. (A) 97% of cells showed no
834 binding of Cy3-labeled colE1-TR to Δ*btuB* (B) ColE1-TR-GFP forms similar puncta as Cy3-
835 labeled ColE1-TR (main text Figure 4C). (C) No binding of Cy3-labeled colE1-T to WT or Δ*tolC*
836 cells was detected with Cy3-labeled colE1-T. Scale bars: 2 μm.
837
838

839 **Fig. S4.**

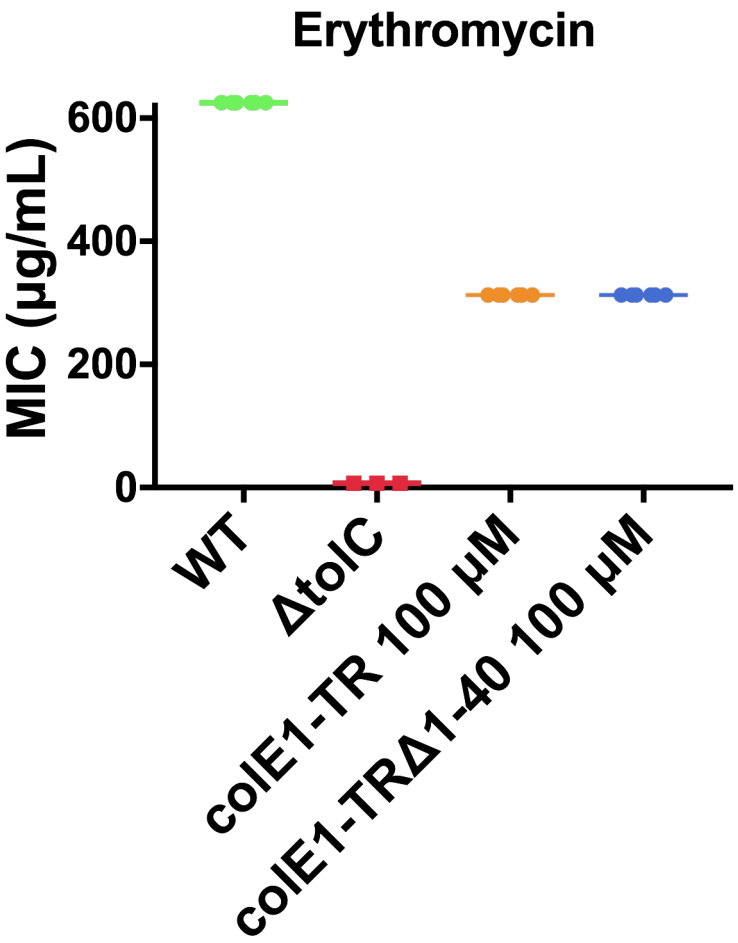

840

841

842 **Figure S4. Minimum Inhibitory Concentration of Erythromycin with colE1-TR TolA box**
843 **deletion construct.** The MIC for erythromycin with 100 µM colE1-TR or colE1-TR$_{\Delta 1\text{-}40}$ is
844 identical indicating that TolA engagement by colE1-TR does not contribute to antibiotic
845 susceptibility.

846

847

848 **Table S1.**

849 Cryo-EM data collection, refinement, and validation statistics

	TolC (EMDB-21960) (PDB 6WXI)	TolC + colE1 (EMDB-21959) (PDB 6WXH)
Data collection and processing		
Electron microscope	Talos Arctica	Talos Arctica
Magnification	130,000×	205,000×
Voltage (kV)	200	200
Electron exposure (e–/Å^2)	33.04	35.96
Defocus range (μm)	0.5-2.6	0.4-2.1
Pixel size (Å)	1.038	0.6578
Symmetry imposed	C_3	C_1 (C_3)
Initial particle images (no.)	2,092,678	339,779
Final particle images (no.)	778,220	179,834
Map resolution (Å)	2.84	3.09 (2.81)
FSC threshold	0.143	0.143
Refinement		
Initial model used (PDB code)	6WXH	1TQQ
Model resolution (Å)	3.11	3.37
FSC threshold	0.5	0.5
R.m.s. deviations		
Bond lengths (Å)	0.0072	0.012
Bond angles (°)	1.11	1.76
Validation		
MolProbity score	1.33	0.50
Clashscore	4.42	0.00
Poor rotamers (%)	1.40	0.18
Ramachandran plot		
Favored (%)	98.12	98.31
Allowed (%)	1.88	1.32
Disallowed (%)	0	0.37

850
851

852 **Table S2.**

853 Mean minimum inhibitory concentrations (MICs) of antimicrobials in the presence of colE1-TR.

854

	Erythromycin (µg/mL)	Ciprofloxacin (ng/mL)	Benzalkonium Chloride (µg/mL)
WT	625.00	56.25	50
Δ*tolC*	7.03	10.16	4.125
WT + 10 µM colE1-TR	312.50	75.00	50
WT + 100 µM colE1-TR	312.50	28.13	25

855

856

857

858

859 **Movie S1.**

860 A representative 8-second movie of colE1-TR bound to a live cell. ColE1-TR localizes on, and
861 remains bound to, the extracellular surface of *E. coli*. Fluorescence movie of Cy3-labeled colE1-
862 TR on living WT *E. coli* overlaid on outline of the *E. coli* cell from phase-contrast microscopy.
863 Continuous imaging at 25 frames per second; the movie plays in real time at the same speed. This
864 movie corresponds to the first 8 seconds of data used to attain the WT image in Figure 4C. Scale
865 bar: 2 µm.

866

867

868

869